Available online at www.sciencedirect.com
ScienceDirect
Journal of Catalysis 247 (2007) 231–237
JOURNAL OF CATALYSIS
www.elsevier.com/locate/jcat

Time-resolved studies on correlations between dynamic electronic structure and selectivity of a $H_5[PV_2Mo_{10}O_{40}]$ partial oxidation catalyst

Thorsten Ressler [a,*], Olaf Timpe [b]

[a] *Technical University Berlin, Institute of Chemistry, Sekr. C 2, Strasse des 17 Juni 135, D-10623 Berlin, Germany*
[b] *Fritz-Haber-Institute of the MPG, Department of Inorganic Chemistry, Faradayweg 4-6, D-14195 Berlin, Germany*

Received 25 August 2006; revised 10 January 2007; accepted 22 January 2007

Available online 8 March 2007

Abstract

Time-resolved in situ X-ray absorption spectroscopy studies on an activated $H_5[PV_2Mo_{10}O_{40}]$ oxidation catalyst were performed to obtain correlations between the dynamic structure and the catalytic selectivity of the material. Both the geometric and electronic structures of the vanadium and molybdenum metal centers of the catalyst change dynamically under the reaction conditions used. Moreover, the selectivity of the catalyst exhibits a pronounced correlation with the degree of reduction and the solid-state kinetics of the reoxidation process. The corresponding extent of reoxidation curve can be simulated with a solid-state kinetic model assuming three-dimensional diffusion as the rate-limiting step. Thus, the partially reduced catalyst exhibits a rate constant of the bulk-diffusion limited reoxidation, coinciding with the temporal evolution of the selectivity of the catalyst.

Keywords: In situ; Heterogeneous catalysis; Structure–activity relationships; Molybdenum; Vanadium; EXAFS spectroscopy; Polyoxometalates; Time-resolution; Dynamic; Solid-state kinetics

1. Introduction

In situ studies on heterogeneous catalysts are indispensable in modern catalysis research. Reliable correlations between the structure of the catalyst and its catalytic performance can be determined only under relevant reaction conditions. These correlations need to be elucidated because they constitute the foundation of a knowledge-based design of novel heterogeneous catalysts [1]. Consequently, many structural analytic techniques, including X-ray absorption spectroscopy (XAS), have been used to study the bulk or surface structure of a catalyst under reaction conditions [2–7]. However, investigating a solid heterogeneous catalyst under steady-state reaction conditions yields little information on the dynamic nature of its surface and bulk structure. Heterogeneous catalysts are metastable materials whose structure and performance change dynamically under reaction conditions. Therefore, time-resolved measurements are needed to further elucidate the behavior of the electronic and geometric structure of a catalyst under changing reaction conditions. Monitoring the gas-phase composition during a catalytic reaction yields conventional kinetic information. Conversely, monitoring bulk structural changes reveals the solid-state kinetics of dynamic structural changes in the bulk of the catalyst under reaction conditions. In combination with simultaneous activity and selectivity measurements by suitable gas-phase analytical techniques, the desired correlations between the catalytic performance and the bulk structure dynamics are obtained.

Heteropolyoxomolybdates of the Keggin type (e.g., $H_3[PMo_{12}O_{40}]$) are active catalysts for the partial oxidation of alkanes and alkenes [8–12]. Because of their molecular structure, heteropolyoxomolybdates of the Keggin type have been frequently used as suitable model systems for more complex molybdenum-based mixed-oxide catalysts. However, the "real" structure of the Keggin ion under reaction conditions is not necessarily identical to the ideal structure of the corresponding as-prepared heteropolyoxomolybdate. In addition to the "ideal" (crystallographic) structure, the "real" structure comprises all deviations from the ideal structure that may be

* Corresponding author. Fax: +49 0 30 314 21106.
E-mail address: thorsten.ressler@tu-berlin.de (T. Ressler).

0021-9517/$ – see front matter
doi:10.1016/j.jcat.2007.01.017

present in the bulk structure of the catalyst. We have recently shown that the onset of catalytic activity during thermal activation of $H_3[PMo_{12}O_{40}]\cdot 13H_2O$ and $H_4[PVMo_{11}O_{40}]\cdot 13H_2O$ in propene coincides with a partial decomposition of the Keggin ion at ∼600 K and migration of Mo centers on extra-Keggin sites [13,14]. Here we report on correlations between the electronic structure and the catalytic selectivity of $H_5[PV_2Mo_{10}O_{40}]\cdot 13H_2O$ under steady-state and dynamic reaction conditions obtained from time-resolved in situ XAS investigations.

2. Experimental

2.1. Preparation of $H_5[PV_2Mo_{10}O_{40}]\cdot 13H_2O$

To begin the preparation, 16.89 g of MoO_3 (corresponding to 11.73 mmol Mo_{10}) and 2.134 g of V_2O_5 (corresponding to 11.73 mmol V_2) were suspended in 650 ml of water in a three-necked 1000-ml flask equipped with a condenser. Commercial phosphoric acid [H_3PO_4 (∼82.5%)] was diluted by a factor of 100, and the exact concentration was determined by titration with NaOH. Then 81 ml of this 0.825% H_3PO_4 solution (11.73 mmol P) was added dropwise to the boiled and stirred suspension of the metal oxides. After complete addition of the phosphoric acid, a clear amber-colored solution was obtained. The solid product was isolated by removing the solvent in a rotary evaporator at ∼90 °C and dried in a vacuum desiccator [15,16]. Thermal analysis studies (TG/DTA-MS) confirmed the amount of ∼13 molecules of "crystal water" per Keggin ion in as-prepared $H_5[PV_2Mo_{10}O_{40}]\cdot 13H_2O$ and a thermal stability similar to that of $H_4[PVMo_{11}O_{40}]\cdot 13H_2O$.

2.2. X-ray diffraction

X-ray diffraction (XRD) measurements were performed on a *STOE STADI P* diffractometer (Cu$K\alpha_1$; Ge primary monochromator) in a range of 5–100° in 2θ with a step width of 0.01° and a measuring time of 10 s/step. Structural refinements to the experimental diffraction patterns were performed using the TOPAS v 2.1 software (Bruker AXS). Structural data used in the XRD and XAS analyses were taken from the Inorganic Crystal Structure Database (ICSD).

2.3. XAS

In situ transmission XAS experiments were performed at the V K-edge (5.465 keV, Si 111) and the Mo K-edge (19.999 keV, Si 311) at beamlines E4 and X1, respectively, at the Hamburg Synchrotron Radiation Laboratory (HASYLAB). The storage ring operated at 4.4 GeV with injection currents of 150 mA. The in situ experiments were conducted in a flow reactor at 1 bar in flowing reactants (flow rate, 30 ml/min; heating rate, 5 K/min to the specified reaction temperature). The gas-phase composition at the cell outlet was continuously analyzed using a noncalibrated mass spectrometer in a multiple-ion detection mode (Omnistar, Pfeiffer).

The heteropolyoxomolybdate was mixed with boron nitride (∼7 mg HPOM and ∼30 mg BN) and pressed with a force of 1 ton into a 5-mm diameter pellet. This resulted in edge jumps of $\Delta\mu_x \sim 1.5$ at the Mo K-edge and $\Delta\mu_x \sim 0.2$ at the V K-edge. $H_5[PV_2Mo_{10}O_{40}]\cdot 13H_2O$ was activated in 10% propene at 300–723 K. Extended XAS studies at the Mo K-edge revealed an intact Keggin structure of the activated $H_5[PV_2Mo_{10}O_{40}]\cdot 13H_2O$. Under isothermal reaction conditions (673, 698, and 723 K), the gas-phase composition was rapidly changed from oxidizing (10% propene and 10% oxygen in He) to reducing (10% propene in He) reaction conditions.

X-ray absorption fine structure (XAFS) analysis was performed using WinXAS version 3.1 software [17]. Background subtraction and normalization were carried out by fitting linear polynomials to the pre-edge and post-edge regions of the absorption spectra, respectively. The extended X-ray absorption fine structure (EXAFS), $\chi(k)$, was extracted using cubic splines to obtain a smooth atomic background, $\mu_0(k)$. The pseudoradial distribution function $FT(\chi(k)k^3)$ was calculated by Fourier transformation of the k^3-weighted experimental $\chi(k)$ function, multiplied by a Bessel window, into the R space. EXAFS data analysis was performed using theoretical backscattering phases and amplitudes calculated with the ab initio multiple-scattering code FEFF7 [18]. Single-scattering and multiple-scattering paths in the Keggin ion model structure were calculated up to 6.0 Å with a lower limit of 2.0% in amplitude with respect to the strongest backscattering path. EXAFS refinements were performed in R space simultaneously with magnitude and imaginary part of a Fourier-transformed k^3- and k^1-weighted experimental $\chi(k)$ using the standard EXAFS formula [19]. The structural parameters determined by a least-squares EXAFS refinement of a Keggin model structure to the experimental spectra are (i) one overall E_0 shift, (ii) Debye–Waller factors for single-scattering paths, (iii) distances of single-scattering paths, and (iv) one-third cumulant for the Mo–O or V–O distances in the first coordination shell and one-third cumulant for all remaining scattering paths. Coordination numbers (CNs) and S_0^2 were kept invariant in the refinement.

3. Results and discussion

This section comprises two parts. The first part establishes that the structure of as-prepared $H_5[PV_2Mo_{10}O_{40}]$ and its structural evolution on thermal activation is similar to that of $H_4[PVMo_{11}O_{40}]$ as described previously [14]. $H_5[PV_2Mo_{10}O_{40}]$ was used because the increased V content makes it more suitable for in situ XAS studies at the V K-edge. The second part of the manuscript describes reversible changes in the local structure around the V centers and the correlation between the time-dependent evolution of the Mo average valence and the catalytic performance of material under rapidly changing reaction conditions (reducing and oxidizing).

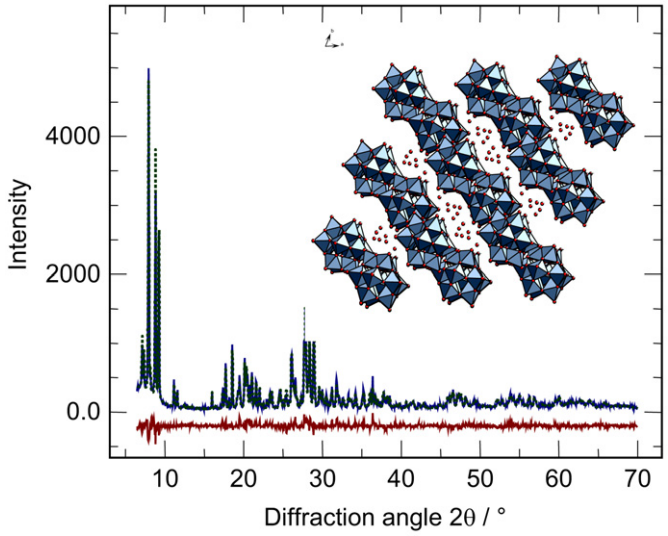

Fig. 1. Experimental (···) and theoretical (—) X-ray diffraction pattern of as-prepared $H_5[PV_2Mo_{10}O_{40}]\cdot 13H_2O$ (P-1, $a = 14.03$ Å, $b = 14.17$ Å, $c = 13.59$ Å, $\alpha = 112.5°$, $\beta = 109.8°$, $\gamma = 60.5°$). The inset shows a schematic structural representation of $H_5[PV_2Mo_{10}O_{40}]\cdot 13H_2O$.

3.1. Characterization and activation of as-prepared $H_5[PV_2Mo_{10}O_{40}]\cdot 13H_2O$

Phase purity and a well-defined long-range order and local structure of the as-prepared $H_5[PV_2Mo_{10}O_{40}]\cdot 13H_2O$ material were confirmed by XRD and XAS measurements. The experimental XRD pattern of the phase pure as-prepared $H_5[PV_2Mo_{10}O_{40}]\cdot 13H_2O$ can be very well simulated with a calculated pattern of $H_3[PMo_{12}O_{40}]\cdot 13H_2O$ [ICSD 31128] (Fig. 1). This confirms that the majority of V centers are located on regular Mo sites in the Keggin ions [14]. $H_5[PV_2Mo_{10}O_{40}]\cdot 13H_2O$ was chosen to obtain an improved XAS signal at the V K-edge. $H_5[PV_2Mo_{10}O_{40}]\cdot 13H_2O$ exhibits a stability comparable to that of $H_4[PVMo_{11}O_{40}]\cdot 13H_2O$ under the conditions used. Conversely, a further increasing V content (V_3 and higher) results in a rapidly decreasing thermal stability of the corresponding polyoxomolybdate [20]. In good agreement with the XRD results, the local structure around the Mo and V centers in as-prepared $H_5[PV_2Mo_{10}O_{40}]\cdot 13H_2O$ can be well described by assuming both metals on regular Mo sites in the Keggin ion (Figs. 2 and 3).

3.2. Characterization of activated $H_5[PV_2Mo_{10}O_{40}]$ under reducing and oxidizing conditions

According to the procedure described previously [14], the as-prepared $H_5[PV_2Mo_{10}O_{40}]\cdot 13H_2O$ was activated by thermal treatment in 10% propene in helium in the temperature range 300–723 K (rate, 5 K/min; dwell time, 10 min at 723 K). In situ XAFS measurements at the Mo K-edge under steady-state reaction conditions yielded the local structure around the Mo centers in activated $H_5[PV_2Mo_{10}O_{40}]$. The local structure corresponded to the characteristically distorted Keggin structure previously reported (i.e., partially decomposed "lacunary" Keggin ions) [14]. XAFS data measured at the V K-edge of

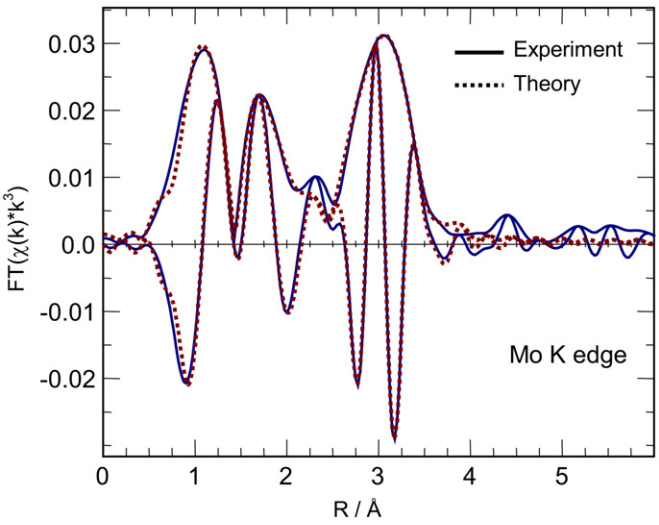

Fig. 2. Experimental (—) and theoretical (- - -) Mo K-edge $FT(\chi(k)k^3)$ (not phase shift corrected) of as-prepared $H_5[PV_2Mo_{10}O_{40}]\cdot 13H_2O$.

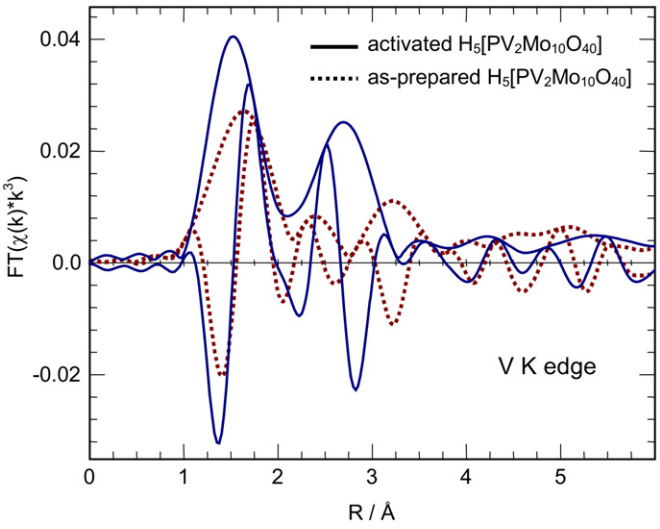

Fig. 3. Experimental V K-edge $FT(\chi(k)k^3)$ (not phase shift corrected) of as-prepared $H_5[PV_2Mo_{10}O_{40}]\cdot 13H_2O$ (- - -) and activated $H_5[PV_2Mo_{10}O_{40}]\cdot 13H_2O$ (—).

activated $H_5[PV_2Mo_{10}O_{40}]$ under steady-state reaction conditions elucidate the geometric and electronic structure of the V centers in the real structure of the active catalyst. Because of the low photon energy of the V K-edge, the required measuring time per spectrum did not permit time-resolved measurements.

When switching the gas phase from reducing (propene) to oxidizing condition (propene and oxygen), evaluation of the characteristic pre-edge peak at the V K-edge yielded an average valence corresponding to 90% V^{4+} and 10% V^{5+} in the reduced state and 70% V^{4+} and 30% V^{5+} in the oxidized state. The average V valence was determined from the height of the pre-edge peak compared with reference samples (V_2O_5, VO_2, V_2O_3) as described previously [21]. The error bar in the absolute average valence amounts to about 0.03 [22], whereas even smaller changes obtained from time-resolved measurements can be analyzed reliably. An average V valence of <5+ in the oxidized

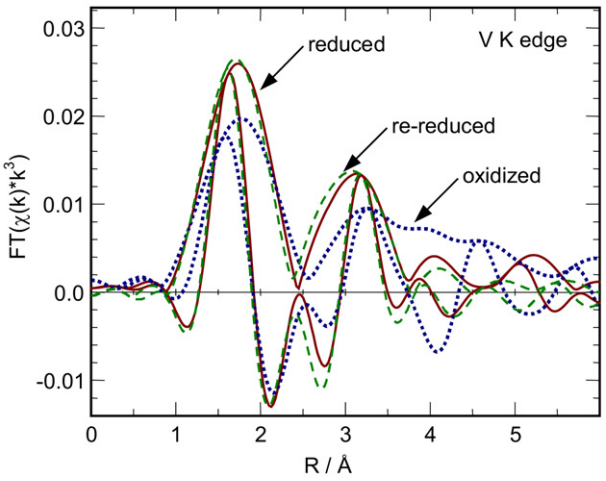

Fig. 4. V K-edge $FT(\chi(k)k^3)$ (not phase shift corrected) of the V centers in activated $H_5[PV_2Mo_{10}O_{40}]\cdot 13H_2O$ in the reduced, oxidized, and re-reduced state.

Table 1
Type and number (N) of atoms at distance R from the V center in the reduced and oxidized state of activated $H_5[PV_2Mo_{10}O_{40}]\cdot 13H_2O$ obtained from a refinement of a Keggin ion model structure (based on V in $K_2H[PMo_{12}O_{40}]\cdot H_2O$, ICSD 209) to the experimental V K-edge XAFS functions $\chi(k)$ (k range from 3.0 to 10 Å^{-1}, R range from 0.9 to 4.0 Å, E_0 (reduced) = 5.06 eV, E_0 (oxidized) = 7.49 eV, residual = 3.0, $N_{ind} = 16$, $N_{free} = 12$). The uncertainty in the distances amounts to about 0.03 Å

Type	N	Model	Reduced state		Oxidized state	
		R (Å)	R (Å)	σ^2 (Å^2)	R (Å)	σ^2 (Å^2)
V–O	1	1.71	1.56	0.0068	1.58	0.0126
V–O	2	1.91	1.97	0.0068	1.98	0.0126
V–O	2	1.92	1.97	0.0068	1.98	0.0126
V–O	1	2.46	2.40	0.0068	2.41	0.0126
V–Mo	**0.6**	**–**	**2.84**	**0.0060**	**3.21**	**0.0091**
V–Mo	2	3.42	3.52	0.0060	3.56	0.0091
V–P	1	3.57	3.49	0.0010	3.42	0.0011
V–Mo	2	3.72	3.72	0.0060	3.80	0.0091

state should be a prerequisite for the V centers to participate in the activation of gas-phase oxygen and propene. Fully oxidized V and Mo centers would not have vacant coordination sites to activate the gas-phase reactants and thus would be catalytically inactive. Conversely, an average V valence between 5+ and 4+ reflects the dynamic behavior of the V valence during the catalytic cycle of propene oxidation.

The local structure around the V center in the reduced state of the activated $H_5[PV_2Mo_{10}O_{40}]$ catalyst corresponded to that of Mo sites in the Keggin ion with an additional short distance to one extra-Keggin Mo center. This structure is similar to that of V centers in the partially decomposed Keggin ion of activated $H_4[PVMo_{11}O_{40}]$. The latter has been described in detail previously [14]. Moreover, the vanadium centers in the lacunary Keggin ions exhibited a dynamic reversible behavior under changing reducing and oxidizing gas-phase potential (Fig. 4). On switching from propene (reducing) to propene and oxygen (oxidizing) and then back to propene, the local structure around the V center changed reversibly from a reduced state to an oxidized state. Whereas the reduced state is characterized by a short vanadium–molybdenum distance of about 2.8 Å, the oxidized state exhibits a longer distance of the vanadium center to the extra-Keggin Mo center of ~3.2 Å (Table 1, Figs. 5a and 5b). The average V valence of <5+ and the significantly reduced amplitude of the $FT(\chi(k)k^3)$ of the vanadium centers in the oxidized state are indicative of a mixture of at least two sites exhibiting slightly different V–O distances around two different V centers (Table 1, Fig. 5b).

3.3. Dynamic behavior of activated $H_5[PV_2Mo_{10}O_{40}]$ under reducing and oxidizing conditions

In addition to studies under steady-state conditions, time-resolved XAFS measurements at the Mo K-edge were performed under changing reaction conditions (time resolution of

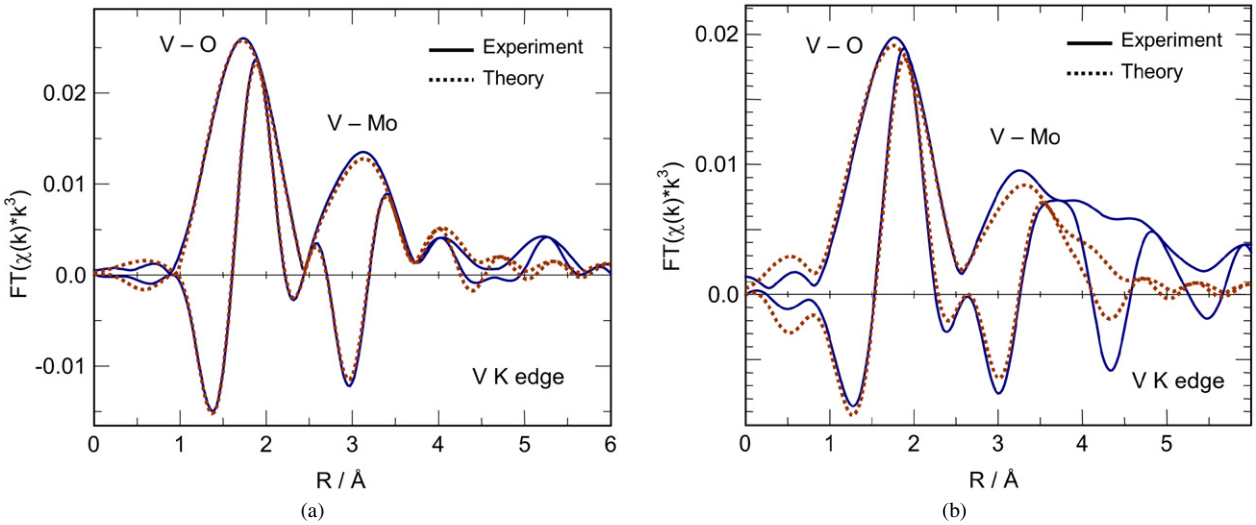

Fig. 5. Theoretical (- - -) and experimental (—) V K-edge $FT(\chi(k)k^3)$ (not phase shift corrected) of the reduced (a) and oxidized (b) state of the V centers in activated $H_5[PV_2Mo_{10}O_{40}]\cdot 13H_2O$.

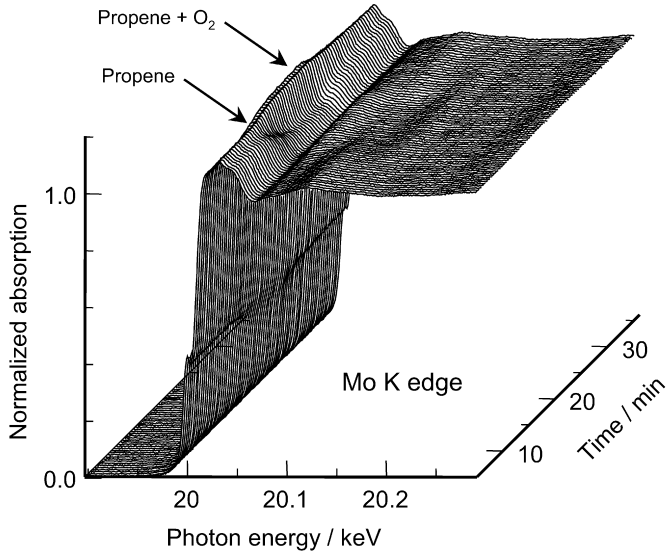

Fig. 6. Evolution of Mo K-edge XANES spectra of activated $H_5[PV_2Mo_{10}O_{40}]\cdot 13H_2O$ during isothermal switching of the gas phase from oxidizing conditions (propene/oxygen) to reducing conditions (propene) and back to oxidizing conditions.

~30 s/spectrum) (Fig. 6). Therefore, the gas-phase composition was isothermally switched from a reducing (propene) to an oxidizing (propene and oxygen) atmosphere (complete exchange in about 20 s in the in situ cell used). The time-resolved XAS investigations allowed us to monitor the structural response of the catalyst on the changing reaction conditions. Analysis of the time-resolved XAS data revealed the solid-state kinetics of the bulk structural changes on reduction and reoxidation of the catalyst. The limited k range available at a sufficient time resolution did not permit a detailed EXAFS analysis of the rapid structural changes. Therefore, we focused on the near-edge region to determine the average Mo valence. The relative Mo K-edge shift was converted into an average Mo valence according to the procedure reported previously [23]. The evolution of the average Mo valence under reducing and oxidizing conditions at various temperatures is depicted in Fig. 7. On switching from propene and oxygen to propene at 673 K, the average Mo valence exhibited a reduction from 6 to 5.94. Assuming spherical particles at a diameter of 100 Å (XRD), an average density of 4.3 g/cm^3, a unit cell constant of the cubic Keggin structure of $a = 11.86$ Å, and about 1 Keggin ion per a^2 at the surface, reduction of one Mo^{6+} site to Mo^{5+} per surface Keggin ion resulted in a total average valence of ~5.94. Apparently at 673 K, the reduction of the Mo centers in the lacunary Keggin ions is mostly limited to the surface of the accessible crystallites. On switching to oxidizing conditions (propene and oxygen) at 673 K, the mostly surface-reduced catalyst was rapidly reoxidized.

Under reducing conditions (propene), increasing reaction temperature was accompanied by a more pronounced decrease in the average valence of the Mo centers in the activated catalyst (Figs. 7b and 7c). The more reduced catalyst at 723 K exhibited a prolonged reoxidation behavior (Fig. 7b). The corresponding extent of the reoxidation curve could be simulated with a

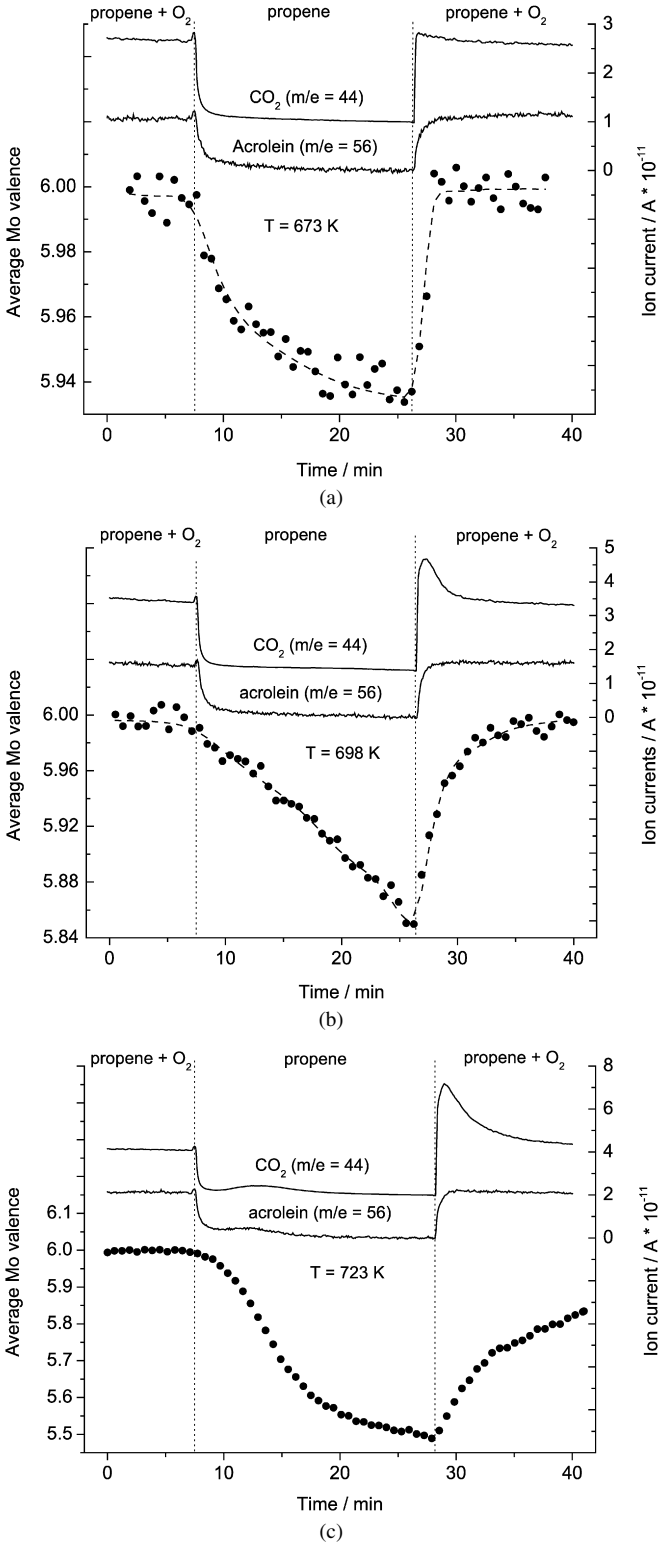

Fig. 7. Evolution of Mo average valence of activated $H_5[PV_2Mo_{10}O_{40}]\cdot 13H_2O$ during changing gas phase composition (propene to propene and oxygen) together with the corresponding evolution of acrolein and CO_2 in the gas phase at 673 (a), 698 (b), and 723 K (c).

solid-state kinetic model assuming three-dimensional diffusion as the rate-limiting step (Fig. 8) [23,24]. An apparent activation energy of about 90 kJ/mol corroborated the assumption of oxygen diffusion limitation in the catalyst bulk.

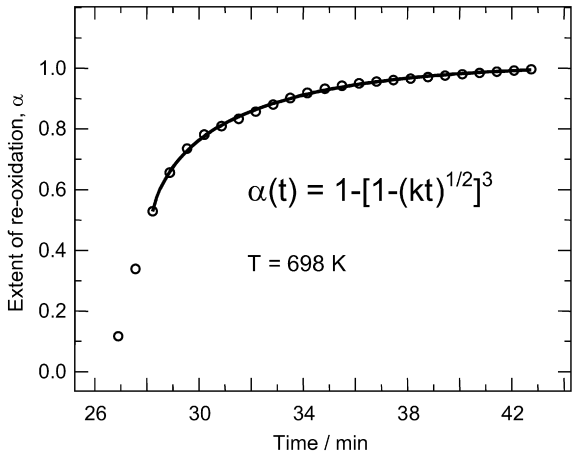

Fig. 8. Refinement of a solid-state kinetic model for three-dimensional solid-state diffusion ($\alpha(t) = 1 - [1 - (kt)^{1/2}]^3$) to the experimental extent of re-oxidation of activated $H_5[PV_2Mo_{10}O_{40}]\cdot 13H_2O$ at 698 K (Fig. 3b).

Intriguingly, the selectivity of the catalyst at the various reaction temperatures exhibited a pronounced correlation with the degree of reduction and the solid-state kinetics of the reoxidation process. After the reductive treatment in propene and a switch back to propene and oxygen at 673 K, the rapid reoxidation of the catalyst was accompanied by a rapid increase in the concentration of both acrolein and CO_2 in the gas phase (Fig. 7a). This indicates that the entirely reoxidized catalyst quickly regained its activity and selectivity in propene oxidation. Conversely, with increasing reaction temperature (698 and 723 K; Figs. 7b and 7c) the partially reduced catalyst exhibited a bulk-diffusion-limited reoxidation rate coinciding with increased production of carbon dioxide and thus reduced selectivity of the catalyst. The production of CO_2 decreased with increasing reoxidation of the catalyst and, after complete reoxidation, reached the same activity and selectivity as before the switching experiments.

The effect of the partially reduced state of the activated $H_5[PV_2Mo_{10}O_{40}]$ catalyst on selectivity is schematically illustrated in Fig. 9. The lower average valence detected during slow reoxidation of the catalyst corresponds to a larger number of V^{4+}–Mo^{5+} sites and oxygen vacancies (Fig. 9, right side). According to the XAFS data, under steady-state conditions, these V^{4+}–Mo^{5+} sites have the characteristic short metal–metal bond of the reduced state of the activated $H_5[PV_2Mo_{10}O_{40}]$ catalyst (Figs. 4 and 9A). Moreover, these V^{4+}–Mo^{5+} sites may be particularly effective in activating gas-phase oxygen, resulting in an oversupply of surface-bond electrophilic oxygen. This electrophilic oxygen is prone to further oxidize propene or acrolein to CO_2 and water [25] (Fig. 9B). On complete catalyst reoxidation, the density of these overactive sites decreases (Fig. 9, left). V^{4+}–Mo^{6+} sites that exhibit a longer metal–metal distance and a lower tendency to form electrophilic oxygen species govern the catalytic performance. Thus, adsorbed propene is mostly oxidized to acrolein by nucleophilic lattice oxygen, and the selectivity of the catalyst increases (Fig. 9C).

The correlation between electronic structure and catalytic performance corroborates the assumption that catalyst selectivity is governed by the electronic structure of the surface. The latter in turn appears to be determined by the electronic defect structure of the underlying bulk [25]. For the activated $H_5[PV_2Mo_{10}O_{40}]$ catalyst studied, reaction conditions that favor a conventional redox mechanism with fast reduction and diffusion-limited reoxidation lead to low selectivity. Conversely, reaction conditions that maintain a rapid reoxidation

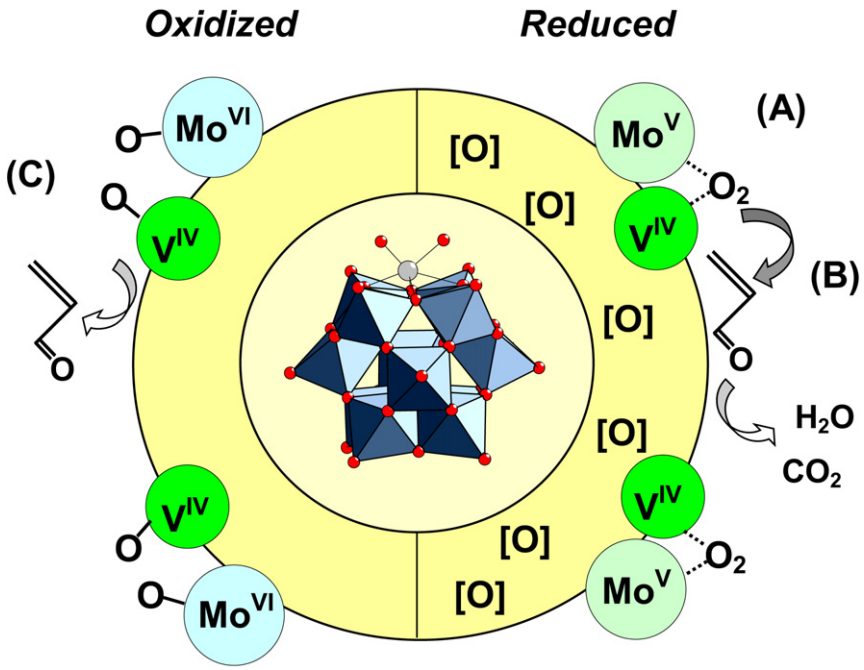

Fig. 9. Schematic representation of the Mo–V local structure of the active site in the reduced (V^{4+}–Mo^{5+}, right) and oxidized (V^{4+}–Mo^{6+}, left) state of activated $H_5[PV_2Mo_{10}O_{40}]\cdot 13H_2O$ in partial oxidation of propene. (A) Electrophilic oxygen species activated by V^{4+}–Mo^{5+} site (right) which (B) result in total oxidation of propene (right). (C) Nucleophilic lattice oxygen on V^{4+}–Mo^{6+} site (left) favoring selective oxidation. [O] denote oxygen vacancies in the bulk (right).

and a small amount of Mo^{5+} centers in the catalyst result in increased selectivity. Consequently, it may be concluded that in a process that involves diffusion of oxygen ions in the catalyst bulk and a prolonged lifetime of partially reduced V^{4+}–Mo^{5+} metal sites, total oxidation of propene will dominate. On the other hand, catalytic oxidation of propene proceeding on an oxidized V^{4+}–Mo^{6+} active site at the surface of the catalyst yields improved selectivity toward partial oxidation products.

4. Conclusion

The time-resolved in situ structural investigations described herein yielded an intriguing correlation between the average valence of the Mo centers in a partial oxidation catalyst, the solid-state kinetics of the reoxidation behavior of the catalyst under dynamic conditions, and the catalytic selectivity. Apparently, the electronic structure of the bulk and of the surface of the catalyst change dynamically under the reaction conditions used, thereby determining the catalytic selectivity of the surface. Moreover, the local structure around the V centers in the proposed active site also exhibits a dynamic behavior as a function of the reduction potential of the gas phase. Correlations between the selectivity of a metal oxide catalyst in partial oxidation reactions and the electronic structure of the corresponding metal centers have been proposed previously based on model assumptions [25]. Nonetheless, experimental data that corroborate these assumptions remain scarce. It emerges that time-resolved bulk structural studies under changing reaction conditions are indeed capable of further elucidating correlations between the dynamic structural behavior of a heterogeneous catalyst and catalytic properties that are not readily available from investigations under steady-state conditions.

Acknowledgment

The authors thank HASYLAB for providing the beamtime for this work.

References

[1] B.L. Kniep, T. Ressler, A. Rabis, F. Girgsdies, M. Baenitz, F. Steglich, R. Schlögl, Angew. Chem. Int. Ed. 43 (2004) 112–115.
[2] F.W.H. Kampers, T.M.J. Maas, J. van Grondelle, P. Brinkgreve, D.C. Koningsberger, Rev. Sci. Instrum. 60 (1989) 2635–2638.
[3] G. Meitzner, S.R. Bare, D. Parker, H. Woo, D.A. Fischer, Rev. Sci. Instrum. 69 (1998) 2618–2621.
[4] B.S. Clausen, K. Grabaek, G. Steffensen, P.L. Hanssen, H. Topsøe, Catal. Lett. 20 (1993) 23–36.
[5] G. Sankar, J.M. Thomas, Top. Catal. 8 (1999) 1–21.
[6] J.D. Grunwaldt, L. Basini, B.S. Clausen, J. Catal. 200 (2001) 321–329.
[7] B.M. Weckhuysen (Ed.), In-situ Spectroscopy of Catalysts, American Scientific Publishers, Los Angeles, 2004, and references therein.
[8] M.M. Lin, Appl. Catal. A Gen. 207 (2001) 1–16.
[9] T. Okuhara, N. Mizuno, M. Misono, Adv. Catal. 41 (2001) 443–673.
[10] M.E. Davis, C.J. Dillon, J.H. Holles, J. Labinger, Angew. Chem. Int. Ed. 41 (2002) 858–860.
[11] J.H. Holles, C.J. Dillon, J.A. Labinger, M.E. Davis, J. Catal. 218 (2003) 42–53.
[12] J.H. Holles, C.J. Dillon, J.A. Labinger, M.E. Davis, J. Catal. 218 (2003) 54–66.
[13] J. Wienold, O. Timpe, T. Ressler, Chem. A Eur. J. 9 (2003) 6007–6017.
[14] T. Ressler, O. Timpe, F. Girgsdies, J. Wienold, T. Neisius, J. Catal. 231 (2005) 279–291.
[15] S. Berndt, D. Herein, F. Zemlin, E. Beckmann, G. Weinberg, J. Schütze, G. Mestl, R. Schlögl, Ber. Bunsen-Ges. Phys. Chem. 102 (1998) 763–774.
[16] G.A. Tsigdinos, Top. Curr. Chem. 76 (1987) 1–64.
[17] T. Ressler, J. Synch. Rad. 5 (1998) 118–122.
[18] J.J. Rehr, C.H. Booth, F. Bridges, S.I. Zabinsky, Phys. Rev. B 49 (1994) 12347–12350.
[19] T. Ressler, S.L. Brock, J. Wong, S.L. Suib, J. Phys. Chem. B 103 (1999) 6407–6420.
[20] O. Timpe, personal communication.
[21] J. Wong, F.W. Lytle, R.P. Messmer, D.H. Maylotte, Phys. Rev. B 30 (1984) 5596–5610.
[22] R.E. Jentoft, A.H.P. Hahn, F.C. Jentoft, T. Ressler, Phys. Chem. Chem. Phys. 7 (2005) 2830–2838.
[23] T. Ressler, R.E. Jentoft, J. Wienold, T. Neisius, J. Catal. 210 (2002) 67–83.
[24] C.H. Bamford (Ed.), Comprehensive Chemical Kinetics, vol. 2, Elsevier, Amsterdam, 1968.
[25] G. Centi, F. Canani, F. Trifiro, in: M.V. Twigg, M.S. Spencer (Eds.), Fundamental and Applied Catalysis, Kluwer Academic/Plenum Publishers, New York, 2001.